Vol. 13, No. 4, 2022
ISSN 2233-4203/ e-ISSN 2093-8950
ARTICLE www.msletters.org | Mass Spectrometry Letters

Analysis of Amyloid Beta 1-16 (Aβ16) Monomer and Dimer Using Electrospray Ionization Mass Spectrometry with Collision-Induced Dissociation

Kyoung Min Kim and Ho-Tae Kim*

Department of Chemistry and Bioscience, Kumoh National Institute of Technology, 61, Daehak-ro, Gumi, Gyeongbuk, 39177, Republic of Korea

Received December 2, 2022, Revised December 12, 2022, Accepted December 12, 2022
First published on the web December 31, 2022; DOI: 10.5478/MSL.2022.13.4.177

Abstract : The monomer and dimer structures of the amyloid fragment Aβ(1–16) sequence formed in H_2O were investigated using electrospray ionization mass spectrometry (MS) and tandem MS (MS/MS). Aβ16 monomers and dimers were indicated by signals representing multiple proton adduct forms, $[monomer+zH]^{n+}$ ($=M^{z+}$, z = charge state) and $[dimer+zH]^{z+}$ ($=D^{z+}$), in the MS spectrum. Fragment ions of monomers and dimers were observed using collision-induced dissociation MS/MS. Peptide bond dissociation was mostly observed in the D1–D7 and V11–K16 regions of the MS/MS spectra for the monomer (or dimer), regardless of the monomer (or dimer) charge state. Both covalent and non-covalent bond dissociation processes were indicated by the MS/MS results for the dimers. During the non-covalent bond dissociation process, the D^{3+} dimer complex was separated into two components: the M^{1+} and M^{2+} subunits. During the covalent bond dissociation of the D^{3+} dimer complex, the b and y fragment ions attached to the monomer, $(M+b_{10-15})^{z+}$ and $(M+y_{9-15})^{z+}$, were thought to originate from the dissociation of the M^{2+} monomer component of the $(M^{1+}+M^{2+})$ complex. Two different D^{3+} complex geometries exist; two distinguished interaction geometries resulting from interactions between the M^{1+} monomer and two different regions of M^{2+} (the N-terminus and C-terminus) are proposed. Intricate fragmentation patterns were observed in the MS/MS spectrum of the D^{5+} complex. The complicated nature of the MS/MS spectrum is attributable to the coexistence of two D^{5+} configurations, $(M^{1+}+M^{4+})$ and $(M^{2+}+M^{3+})$, in the Aβ16 solution.

Keywords : Aβ16, Aβ16 dimer, collision-induced dissociation, mass spectrometry, MS/MS

Introduction

An understanding of protein misfolding is crucial to understanding the pathology of neurodegenerative diseases. One example of a misfolded protein is Aβ in Alzheimer's disease (AD).[1,2] AD is characterized by the extracellular deposition of Aβ in the form of plaques and neurofibrillary tangles of the Tau protein in the brain.[3,4] In the plaque deposition of Aβ, Aβ oligomers that formed in the early stage of Aβ aggregation are considered to be the most neurotoxic agents in AD.[5-8] However, the structure and formation process of Aβ oligomers are not yet understood clearly because of the metastable character of Aβ oligomers.[9]

Accordingly, oligomer formation processes have been studied using various experimental and theoretical methods including ion-mobility mass spectrometry,[10,11] CD,[12,13] NMR experiments[14,15] and computer simulations.[16-20] The collision cross-sections and the percentage of β-strands or α-helix content of oligomers were reported to aid in understanding or inhibiting Aβ fibril formation process. One (residues 12–24), two (residues 12–24 and 30–42), or three (1–6, 12–24, and 30–42) active regions were reported as critical interaction areas in the Aβ42 aggregation process.[14,21-23] Several stable dimer conformations were also reported in a simulation study of Aβ oligomer.[19,20]

Short Aβ fragments (Aβ16–20, Aβ35–40, Aβ1–16, Aβ17–42, and Aβ1–28) have been studied to aid in understanding (or inhibiting) the Aβ aggregation process.[24-28] However, the exact sequence of aggregation events and their role remain unclear. In particular, reports of the Aβ16 fragment, which is regarded as a potential inhibitor[29,30] of Aβ aggregation, are discrepant. Some studies[31,32] reported that Aβ16 fragments do not aggregate and reduce Aβ16 cytotoxicity in neuronal cells, whereas other reports state that Aβ16 aggregates and Aβ16 oligomers are cytotoxic.[26,33] These conflicting experimental results were obtained using

*Reprint requests to Ho-Tae Kim
https://orcid.org/0000-0002-1541-3081
E-mail: hotaekim@kumoh.ac.kr

various experimental techniques. Metal (Ni, Cu, Zn, and Al, among others) ion-induced Aβ16 aggregation was also studied to understand the reactivity and functional group activity of Aβ16. The 10–16 residue region of Aβ appears to be an effective metal ion trapping unit.[34,35] His6 and other carbonyl groups have also been reported as potential active regions for the metal ion binding unit.

In this study, we used collision-induced dissociation (CID) in conjunction with electrospray ionization (ESI)-mass spectrometry (MS) to obtain structural information on the Aβ16 monomer and dimer. Aβ16 dimer complexes were allowed to form in solution and were electrosprayed onto a quadrupole ion guide. ESI-MS was assumed to produce intact gas-phase dimer complex ions from the Aβ16 dimer complex in solution. A low-energy CID-tandem MS (MS/MS) method was applied to investigate the fragment ion species and patterns of the multiply charged monomers and dimers of Aβ16.

Experimental

The MS and MS/MS spectra for the Aβ16 fragmentation pattern analysis were obtained using a Thermo Finnigan LTQ mass spectrometer (Thermo Fisher Scientific, Waltham, MA, USA), which is a linear ion trap mass spectrometer equipped with an atmospheric pressure ESI source.

MS conditions

Aβ16 samples (in H_2O) were introduced to the ESI interface via a direct infusion method using a microsyringe pump (Hamilton, USA) at a flow rate of 1 mL/min. The CID-MS/MS experiments were conducted at capillary temperatures of 150°C, which resulted in the best signal-to-noise ratios for the MS/MS spectra. The positive ion MS spectra were acquired over an *m/z* range of 100–2000 by averaging 1000–4000 scans. The MS/MS experimental conditions were as follows: ion-trap pressure, 1×10^{-5} Torr; activation time, 30 ms; injection time, 100–200 ms; and isolation width, 0.8–1.5 mass units. The parent Aβ16 ions were individually and manually selected and subjected to CID. The collision energies were optimized for each MS/MS experiment to obtain sufficient signal-to-noise ratios.

Reagents

The Aβ16 peptide, synthetic peptide (purity > 95%), amidated at the C-terminus (DAEFRHDSGYEVHHQK-NH_2, Peptron, Daejeon, Korea), and HPLC-grade H_2O (Merck Ltd., Korea) were used in the experiments. Aβ16 peptides were dissolved in H_2O to prepare 150 μM solutions. Solutions were prepared to achieve sufficient D^{5+} ion intensity in the CID-MS/MS experiments. The experiments were performed within 24 h of sample preparation.

Results and Discussion

MS Spectra

Under our ESI experimental conditions, the mass spectra of the Aβ16 solutions indicated the presence of multiply charged monomers and oligomers (Figure 1). Aβ16 monomers were observed at *m/z* 1953.9, 977.5, 652.0, and 489.2, ranging from 1+ to 4+ and $[M+H^+]$ to $[M+4H^+]$ as multiple proton adducts forms. The Aβ16 peptide contains five basic residues (Arg5, His6, His13, His14, and Lys16) and an N-terminal position available for protonation. There are also four acidic residues (Asp1, Glu3, Asp7 and Glu11) in the Aβ16 peptide. The M^{5+} peak at *m/z* 391.6 was not observed in the ESI-MS spectrum of the Aβ16 solution (Figure 1). The M^{3+} monomer peak was observed with a

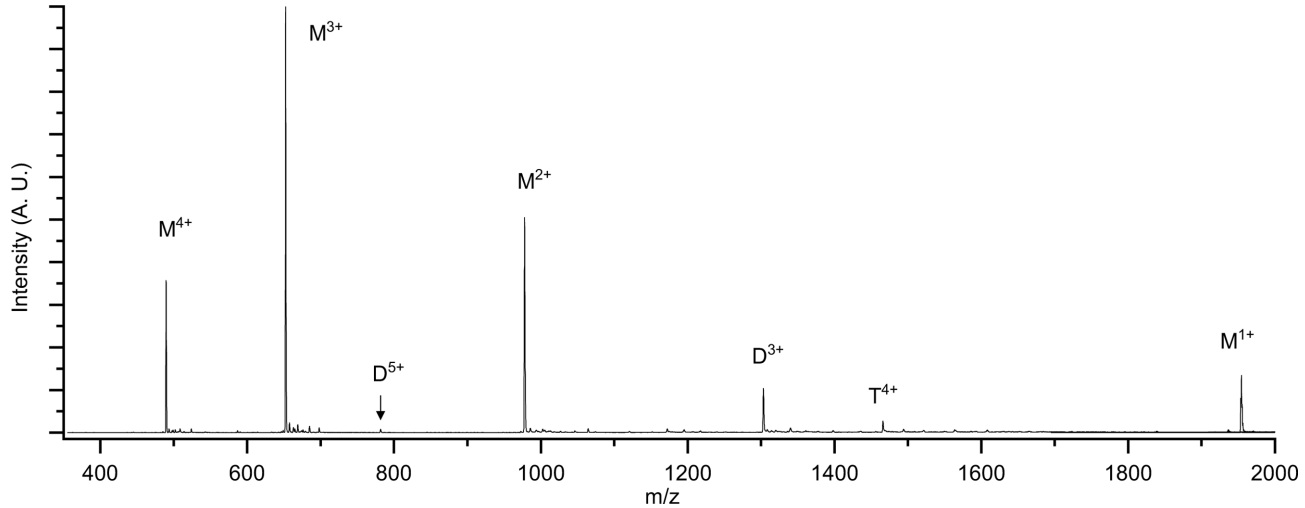

Figure 1. ESI-MS spectrum of Aβ16 solution. Multiply charged monomers and oligomers are represented as M^{z+}, D^{z+}, and T^{z+} (M = monomer, D = dimer, T = trimer, and z = charge state).

high-intensity peak. For the oligomers, peaks were observed at *m/z* 1302.9, 782.2, and 1465.7, corresponding to D^{3+}, D^{5+}, and T^{4+} (T=trimer), respectively.

MS spectra of the Aβ16 peptide have been reported in previous studies.[36-38] Oligomer complexes were not observed in these spectra because of the Aβ16 concentrations and experimental conditions. The positive charge state distribution of the Aβ16 monomers (Figure 1) is consistent with that of the previously reported MS spectrum. The new observation of D^{3+}, D^{5+}, and T^{4+} complexes indicated the possibility of aggregation of the Aβ16 peptides. The aggregation process of Aβ16 might be different from that of Aβ protein because of the extra Aβ17-42 peptide region. The configurations (up to trimer) and *m/z* values of the observed complexes are listed in the Supplementary Information Table S1.

MS/MS spectra of monomers

CID-MS/MS experiments were conducted to obtain structural information regarding the parent Aβ16 monomer and dimer ions. The MS/MS spectra of Aβ16 monomers are shown in Figure 2 and 3. The fragment ions were labeled with various colors and shapes based on the charge states and fragment ion species in Figure 2 and 3. The *m/z* values and assignments for the fragment ions in Figure 2 and 3 are presented in the Supplementary Information Table S2. These monomer MS/MS fragmentation patterns are useful for analyzing the dimer MS/MS spectrum, according to the charge state. The similar fragment ions of M^{2+}, M^{3+}, and M^{4+} monomers have been reported under different experimental conditions (in CH_3OH:H_2O 97:3 solution).[36] The MS/MS fragment ion species shown in Figure 2 and 3 are similar to those of previously reported spectra. However, some fragment ions observed in this study have not been reported previously (including b_{13}^{3+}, b_{14}^{3+}, b_{15}^{3+}, shown in Figure 2b, y_{13}^{3+}, b_9^{2+}, shown in Figure 3a, and y_{14}^{3+}, shown in Figure 3b). In the MS/MS spectrum for Aβ16 M^{1+} and M^{2+} (Figure 2), we observed high-intensity fragment ions at the peptide bonds of the N-terminus (D1–D7) and C-terminus (V11–K16) region. The peptide bond dissociation between D7 and S8, corresponding to the b_7 and y_9 ions, was also observed as another characteristic dissociation channel in the CID process of M^{1+} or M^{2+} parent ions. The dissociation process in the central region, residues S8–Y10, cannot be observed in the monomer spectra (Figure 2). However, we observed distinctive fragment ions, originating from the S8–Y10 central region, in the MS/MS spectrum of M^{3+} (Figure 3a). The (b_8^{2+}–b_{10}^{2+}) fragment ions were observed by a part of the (2+) b_u ion series peaks at u = 7–15. The (2+) b_u ion series peaks at u = 7–15, which were observed at high intensities, are the characteristic ion series observed in the MS/MS spectrum of M^{3+} (Figure 3a). These ion series were only observed in the MS/MS spectrum of M^{3+} among four monomer parent ions (M^{1+}–M^{4+}). The b or y fragment ions from the peptide bonds of the N-terminus and C-

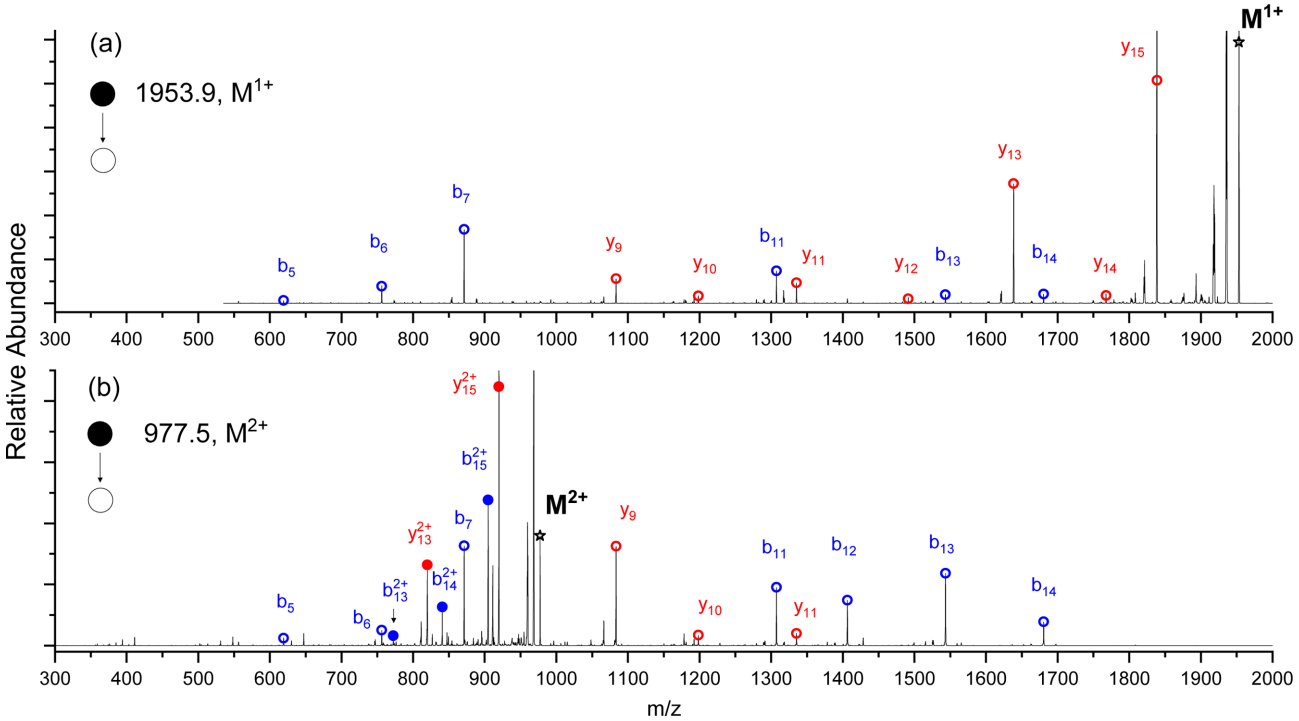

Figure 2. MS/MS spectra of monomers of Aβ16 (a) M^{1+} and (b) M^{2+}. (1+) b fragment ions are indicated by blue empty circle and (1+) y fragment ions are indicated by red empty circle at top of peak. (2+) b and y fragment ions are indicated by filled circles.

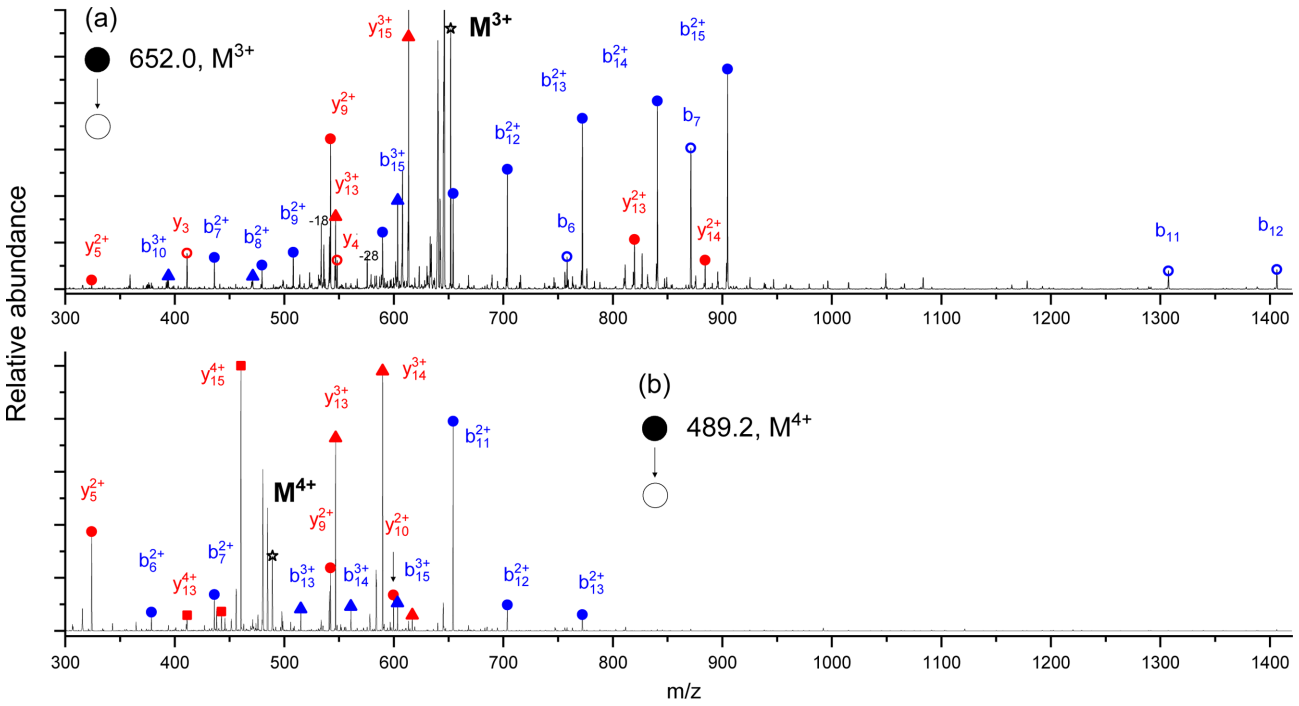

Figure 3. MS/MS spectra of (a) M^{3+} and (b) M^{4+} monomers. (1+) b fragment series peaks are indicated by empty blue circles and (1+) y fragment series peaks are indicated by empty red circles at top of peak. (2+) b and y fragment ions are indicated by filled circles, (3+) b and y fragment ions by filled triangles, and (4+) b and y fragment ions by filled squares at top of peak.

Table 1. Comparison of MS/MS fragment ions of Aβ16 monomers and dimers. b and y ions were observed in MS/MS spectrum for monomers and b, y, (M+ b), and (M+ y) fragment ions were observed in MS/MS spectrum for dimers.

Parent ion	Observed MS/MS fragment ions		
	residue 1-7	residue 8-10	residue 11-16
M^{1+}	b_5^{1+} - b_7^{1+} // y_{15}^{1+} - y_9^{1+}		b_{11}^{1+} - b_{14}^{1+}
M^{2+}	b_5^{1+} - b_7^{1+} y_{11}^{1+} - y_9^{1+} // y_{15}^{2+} - y_{13}^{2+}		b_{11}^{1+} - b_{14}^{1+} // b_{13}^{2+} - b_{15}^{2+}
M^{3+}	b_5^{1+} - b_7^{1+} b_7^{2+}, y_{14}^{2+}, y_{13}^{2+} y_{15}^{3+}, y_{13}^{3+}	b_8^{2+} - b_{10}^{2+} b_{10}^{3+}	b_{11}^{1+} - b_{12}^{1+} // y_4^{1+} - y_3^{1+} << b_{11}^{2+} - b_{15}^{2+} >> b_{12}^{3+}, b_{15}^{3+}
M^{4+}	b_6^{2+} - b_7^{2+} < y_{14}^{3+}, y_{13}^{3+} > y_{15}^{4+} - y_{13}^{4+}		b_{11}^{2+} - b_{13}^{2+}, y_5^{2+} - y_3^{2+} b_{13}^{3+} - b_{15}^{3+}
D^{3+}	b_5^{1+} - b_7^{1+} $[M+y_{11}]^{2+}$ - $[M+y_9]^{2+}$ // $[M+y_{15}]^{3+}$ - $[M+y_{13}]^{3+}$		$[M+b_{11}]^{2+}$ - $[M+b_{14}]^{2+}$
D^{5+}	b_7^{1+} $[M+y_{11}]^{3+}$ - $[M+y_9]^{3+}$ < $[M+y_{14}]^{4+}$, $[M+y_{13}]^{4+}$ > $[M+y_{15}]^{5+}$ - $[M+y_{13}]^{5+}$	 $[M+b_{10}]^{5+}$	b_{11}^{1+}, b_{12}^{1+} // b_{11}^{2+}, b_{12}^{2+} // y_4^{1+} $[M+b_{11}]^{3+}$ - $[M+b_{13}]^{3+}$ << $[M+b_{11}]^{4+}$ - $[M+b_{15}]^{4+}$ >> $[M+b_{12}]^{5+}$, $[M+b_{15}]^{5+}$

terminus regions are also observed in Figure 3 with (+1) to (+4) charge states. The observed fragment ions are listed in Table 1.

MS/MS spectra of the dimers

Both covalent and non-covalent bond dissociation were indicated by the MS/MS spectra of the dimers (Figure 4).

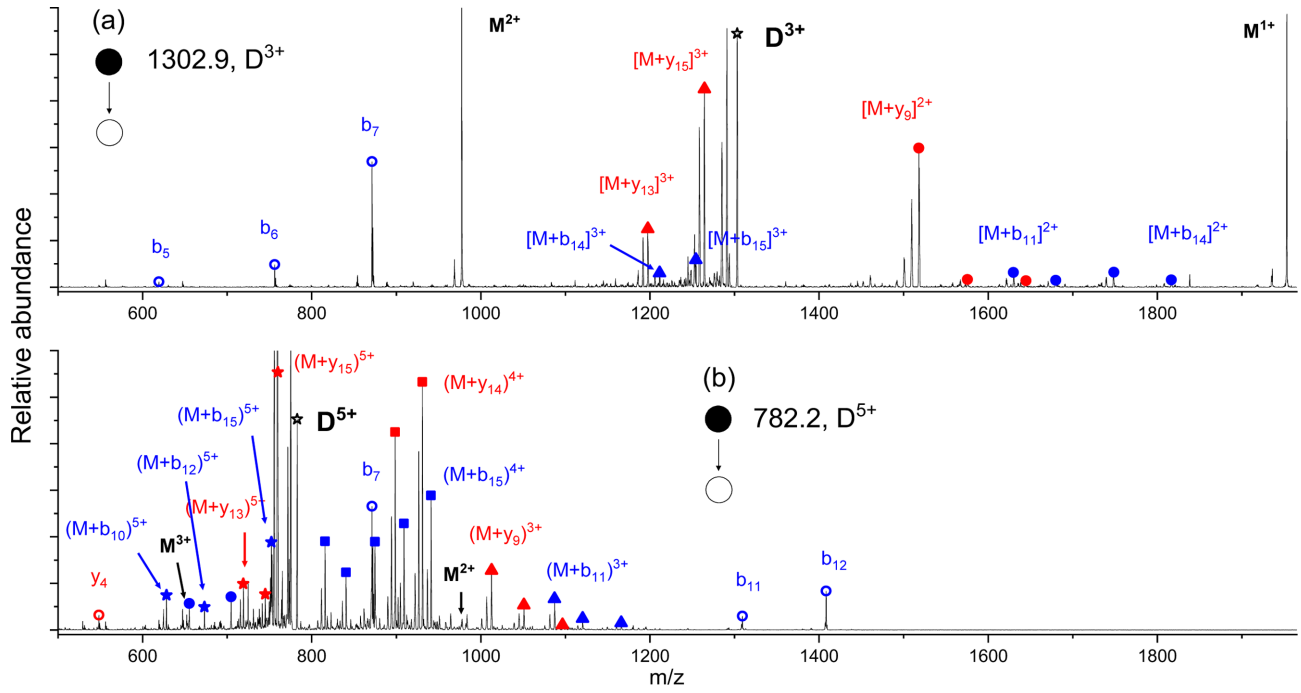

Figure 4. MS/MS spectra of Aβ16 (a) D^{3+} parent ion and (b) D^{5+}. [M+ b, y ions]$^{4+}$ fragment ions are indicated by blue or red filled squares, [M+ b, y ions]$^{3+}$ by blue or red filled triangles, [M+ b, y ions]$^{2+}$ by blue or red filled circles, and [b, y ions]$^{1+}$ by blue or red empty circles at top of peaks.

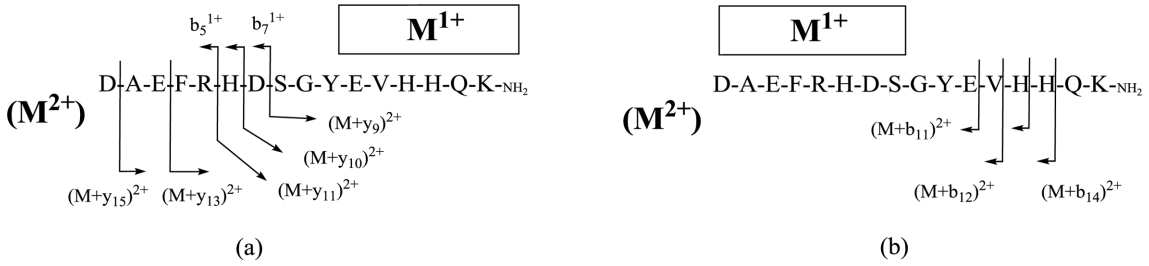

Scheme 1. Schematics of proposed Aβ16 D^{3+} complex. M^{1+} monomer interacts at (a) the C-terminus region of M^{2+} monomer and (b) N-terminus region of M^{2+} monomer.

During the non-covalent bond dissociation process, the D^{3+} dimer complex was separated into two components, M^{1+} and M^{2+}, which produced high-intensity peaks (Figure 4a). The D^{3+} complex is most likely composed of (M^{1+}+M^{2+}), rather than (M^{0}+M^{3+}) complex geometry. In the case of the D^{5+} complex, M^{2+} and M^{3+} subunits were indicated by low-intensity peaks under our low-energy CID conditions (Figure 4b). However, the non-covalent bond dissociation resulted in the peak of the M^{1+} or M^{4+} subunit ions was not observed in Figure 4b. The charge state of parent ion is most likely crucial to the non-covalent bond dissociation process under our low-energy CID conditions. The possibility of the conformational change could also be existed in the CID thermal energy process.

During the covalent bond dissociation process, the D^{3+} MS/MS spectrum (Figure 4a) showed three fragment ion series, ① singly charged b_5–b_7 ions, ② doubly or triply charged $[(M^{1+})+b_{11}]^{2+}$–$[(M^{1+})+b_{14}]^{2+}$ and $[(M^{1+})+b_{14}]^{3+}$ –$[(M^{1+})+b_{15}]^{3+}$ ions, and ③ doubly or triply charged $[(M^{1+})+y_{11}]^{2+}$–$[(M^{1+})+y_{9}]^{2+}$ and $[(M^{1+})+y_{15}]^{3+}$–$[(M^{1+})+y_{13}]^{3+}$ fragment ions. The fragmentation patterns of the ①, ②, and ③ series are exactly the same as those shown in the M^{2+} MS/MS spectrum (Figure 2b), except for (M^{1+}) component in the ② and ③ fragment ion series. Therefore, it is expected that the observed CID-MS/MS fragmentation pattern shown in Figure 4a originates from the M^{2+} monomer component of the (M^{1+}+M^{2+}) dimer geometry. The entire M^{1+} component is completely conserved throughout the MS/MS dissociation of the D^{3+} complex.

The two proposed Aβ16 D^{3+} structures are shown in Scheme 1, based on observations of the ①, ②, and ③ ion series. The two proposed geometric configurations of the

D^{3+} complex presumably coexist in the Aβ16 solution. The D^{3+} complex geometry shown in Scheme 1a is a likely candidate to explain the series ① or ③ fragment ion patterns, whereas the Scheme 1b geometry explains the series ② fragment ion patterns.

The Scheme 1b geometry of D^{3+} complex is not appropriate for explaining the singly charged b_5–b_7 ions in ① pattern because the fragile R5–D7 region of M^{2+} is blocked by the attachment of M^{1+}, which inhibits the dissociation of the fragile R5–D7 region of M^{2+}. Judging from the common observation of singly or doubly charged b_5–b_7 ions in the MS/MS spectra of M^{1+}–M^{4+}, the R5–D7 region is prone to dissociation in the Aβ16 complex.

Therefore, it is deduced that the singly charged b_5–b_7 ions in ① pattern were resulted from the Scheme 1a geometry of D^{3+} complex because there is no interaction between M^{1+} component and the fragile R5–D7 region of M^{2+}. The possible dissociation channels are indicated by arrows in Scheme 1. If the M^{1+} component is attached to the restricted D1–F4 region of M^{2+} in the Scheme 1b geometry, the singly charged b_5–b_7 ions of ① pattern could be differently observed, resulted in the $[M^{1+}+b_5]$–$[M^{1+}+b_7]$ attached ions. However, the attached fragment ions $[M^{1+}+b_5]$–$[M^{1+}+b_7]$ were not observed in the D^{3+} MS/MS spectrum (Figure 4a).

Notably, fragment ion series ② in the D^{3+} MS/MS spectrum is low intensity. The intensities of the $[M+b_{11}]^{2+}$–$[M+b_{14}]^{2+}$ and $[M+b_{14}]^{3+}$–$[M+b_{15}]^{3+}$ monomer attached ions were significantly lower than those of ($b_{11}{}^{1+}$–$b_{14}{}^{1+}$) and ($b_{14}{}^{2+}$–$b_{15}{}^{2+}$), as shown in Figure 2b.

In fragment ion series of ③ pattern, the $[M+y_9]^{2+}$ ion is a counter ion to the $b_7{}^{1+}$ fragment ion in the D7–S8 peptide bond dissociation process of the D^{3+} complex illustrated in Scheme 1a. The high intensities of the $[M+y_9]^{2+}$ and $b_7{}^{1+}$ ions suggested that the D7–S8 peptide bond is one of the weak bonds in the D^{3+} complex of Scheme 1a, similar to how the D7–S8 peptide bond is one of the weak bonds in the M^{2+} monomer.

According to the difference in the intensities of ② and ③ patterns (Figure 4a), it is presumed that the complex formation efficiency of Scheme 1a geometry is better than that of Scheme 1b geometry. Consequently, we believe that the geometry proposed in Scheme 1a is the major species of D^{3+} complex in the Aβ16 solution.

In the MS/MS spectrum of the D^{5+} complex (Figure 4b), intricate fragmentation patterns resulting from the covalent bond dissociation process were observed. Two characteristic fragmentation patterns are observed in Figure 4b, ④ $[(M^{1+})+(y_{13}{}^{3+})]^{4+}$ and $[(M^{1+})+(y_{14}{}^{3+})]^{4+}$ and ⑤ $[(M^{2+})+(b_{11}{}^{2+})]^{4+}$–$[(M^{2+})+(b_{15}{}^{2+})]^{4+}$ fragment ions. The fragment ion series and intensities of ④ pattern or ⑤ pattern are consistent to those of the M^{4+} or M^{3+} spectrum (Figure 3) except (M^{1+}) or (M^{2+}) monomer attachment in the ④ and ⑤ fragment ions. Therefore, the fragment ions of ④ pattern were assigned to the fragments resulting from the dissociation of the M^{4+} monomer component of the (M^{1+}+M^{4+}) dimer geometry and the fragment ions of ⑤ pattern were assigned to those resulting from the dissociation of the M^{3+} monomer component of the (M^{2+}+M^{3+}) dimer geometry.

The triply charged ⑥ $[M+y_{11}]^{3+}$–$[M+y_9]^{3+}$ and $[M+b_{11}]^{3+}$–$[M+b_{13}]^{3+}$ ion signals are commonly attributable to fragments resulting from the dissociation of the M^{4+} component in the (M^{1+}+M^{4+}) or M^{3+} component of the (M^{2+}+M^{3+}) dimer geometry.

However, the ⑦ ($b_7{}^{1+}$, $b_{11}{}^{1+}$, and $b_{12}{}^{1+}$) ion signals are attributable to the fragments resulting from the dissociation of the M^{3+} monomer component of the (M^{2+}+M^{3+}) dimer geometry. The ($b_7{}^{1+}$, $b_{11}{}^{1+}$, and $b_{12}{}^{1+}$) fragment ion signals were not observed in the MS/MS spectrum for M^{4+} (Figure 3b). The two proposed D^{3+} structures (Schemes 1a and 1b) are still applicable to the D^{5+} structures with different combinations of (M^{1+}+M^{4+}) or (M^{2+}+M^{3+}) dimer geometries. Judging from the similar intensities of the signals in ④ and ⑤ patterns, no geometric preference for either (M^{1+}+M^{4+}) or (M^{2+}+M^{3+}) configurations was indicated.

Conclusion

CID-MS/MS experiments were conducted to obtain structural information regarding of the Aβ16 dimer complex. The D^{3+} complex is composed of two subunits, M^{1+} and M^{2+}. The Scheme 1a geometry of D^{3+} complex was expected to be more favorable than the Scheme 1b geometry. The b and y fragment ions attached to the monomer, $(M+ b_{10\text{-}15})^{z+}$ and $(M+ y_{9\text{-}15})^{z+}$, were believed to originate from the dissociation of the M^{2+} monomer component of the (M^{1+}+M^{2+}) dimer geometry. Intricate fragmentation patterns were observed in the MS/MS spectrum of the D^{5+} complexes. The complicated nature of the MS/MS spectrum is attributable to the coexistence of two D^{5+} configurations, (M^{1+}+M^{4+}) and (M^{2+}+M^{3+}), in the Aβ16 solution.

Acknowledgments

This study was supported by the Research Fund of the Kumoh National Institute of Technology (202002270001).

Notes and references

Electronic Supplementary Information is available: [Details of any available supplementary information should be included here]. See DOI: xx.xxxx/xxxxx./

References

1. Chiti, F.; Dobson, C. M. *Annu. Rev. Biochem.* **2006**, 75, 333. DOI: 10.1146/annurev.biochem.75.101304.123901

2. Shankar, G. M.; Walsh, D. M. *Mol. Neurodegener.* **2009**, 4, 48. DOI:10.1186/1750-1326-4-48
3. Selkoe, D. J. *Physio.l Rev.* **2001**, 81, 741. DOI: 10.1152/physrev.2001.81.2.741
4. Brunden, K. R.; Trojanowski, J. Q.; Lee, V. M.-Y. *Nat. Rev. Drug Discov.* **2009**, 8, 783. DOI: 10.1038/nrd2959.
5. Kirkitadze, M. D.; Bitan, G.; Teplow, D. B. *J. Neurosci. Res.* **2002**, 69, 567. DOI: 10.1002/jnr.10328
6. Klein, W. L.; Stine, W. B.; Teplow, D. B. *Neurobiol. Aging* **2004**, 25, 569. DOI: 10.1016/j.neurobiolaging.2004.02.010
7. Haass, C.; Selkoe, D. J. *Nat. Rev. Mol. Cell Biol.* **2007**, 8, 101. DOI: 10.1038/nrm2101
8. Sengupta, U.; Nilson, A. N.; Kayed, R. *EBioMedicine* **2016**, 6, 42. http://dx.doi.org/10.1016/j.ebiom.2016.03.035
9. Benilova, I.; Karran, E.; De Strooper, B. *Nat. Neurosci.* **2012**, 15, 349. DOI: 10.1038/nn.3028
10. Pujol-Pina, R.; Vilaprinyó-Pascual, S.; Mazzucato, R.; Arcella, A.; Vilaseca, M.; Orozco, M.; Carulla, N. *Scientific Reports* **2015,** 5, 14809. DOI: 10.1038/srep14809
11. Bernstein, S. L.; Dupuis, N. F.; Lazo, N. D.; Wyttenbach, T,; Condron, M. M.; Bitan, G.; Teplow, D. B.; Shea, J.-E.; Ruotolo, B. T.; Robinson, C. V.; Bowers, M. T. *Nat. Chem.* **2009**, 1, 326. DOI: 10.1038/nchem.247
12. Kirkitadze, M. D.; Condron, M. M.; Teplow, D. B. *J. Mol. Biol.* **2001**, 312, 1103. DOI: 10.1006/jmbi.2001.4970
13. Ono, K.; Condron, M. M.; Teplow, D. B. *Proc. Natl. Acad. Sci. U.S.A.* **2009**, 106, 14745. DOI: 10.1073/pnas.0905127106
14. Petkova, A. T.; Yau, W.-M.; Tycko, R. *Biochemistry* **2006**, 45, 498. DOI: 10.1021/bi051952q
15. Paravastu, A. K.; Leapman, R. D.; Yau, W.-M.; Tycko, R. *Proc. Natl. Acad. Sci.* **2008**, 105, 18349. DOI: 10.1073/pnas.0806270105
16. Chong, S.-H.; Ham, S. *Phys. Chem. Chem. Phys*. **2012**, 14, 1573. DOI: 10.1039/c2cp23326f
17. Zhang, T.; Zhang, J.; Derreumaux, P.; Mu, Y. *J. Phys. Chem. B* **2013**, 117, 3993. DOI: 10.1021/jp312573y
18. Das, P.; Chacko, A. R.; Belfort, G. *ACS Chem. Neurosci.* **2017**, 8, 606. DOI: 10.1021/acschemneuro.6b00357
19. Barz, B.; Liao, Q.; Strodel, B. *J. Am. Chem. Soc*. **2018**, 140, 319. DOI: 10.1021/jacs.7b10343
20. Zou, Y.; Qian, Z.; Chen, Y.; Qian H.; Wei, G.; Zhang, Q. *ACS Chem. Neurosci.* **2019**, 10, 1585. DOI: 10.1021/acschemneuro.8b00537
21. Reinke, A. A., Ung, P. M., Quintero, J. J., Carlson, H. A. & Gestwicki, J. E. *J. Am. Chem. Soc.* **2010**, 132, 17655. DOI: 10.1021/ja106291e
22. Ahmed, M.; Davis, J.; Aucoin, D.; Sato, T.; Ahuja, S.; Aimoto, S.; Elliott, J. I.; Van Nostrand, W. E.; Smith, S. O. *Nat. Struct. Mol. Biol.* **2010**, 17, 561. DOI: 10.1038/nsmb.1799
23. Haupt, C.; Leppert, J.; Rçnicke, R.; Meinhardt, J.; Yadav, J. K. *Angew. Chem. Int. Ed. Engl.* **2012**, 51, 1576. DOI: 10.1002/anie.201105638
24. Castelletto, V.; Ryumin, P.; Cramer, R.; Hamley, I. W.; Taylor, M.; Allsop, D.; Reza, M.; Ruokolainen, J.; Arnold, T.; Hermida-Merino, D.; Garcia, C. I.; Leal, M. C.; Castaño, E. *Scientific Reports* **2017**, 7, 43637. DOI: 10.1038/srep43637
25. Berhanu, W. M.; Masunov, A. E. *J. Mol. Model* **2011**, 17, 2423. DOI: 10.1007/s00894-010-0912-4
26. M. Shabestari, M.; Plug, T.; Motazacker, M. M.; Meeuwenoord, N. J.; Filippov, D. V.; Meijers, J. C. M.; Huber, M. *Appl. Magn. Reson.* **2013**, 44, 1167. DOI: 10.1007/s00723-013-0469-3
27. Kuhn, A. J.; Abrams, B. S.; Knowlton, S.; Raskatov, J. A. *ACS Chem. Neurosci.* **2020**, 11, 1539. DOI: 10.1021/acschemneuro.0c00160
28. Jiang, D.; Men, L.; Wang, J.; Zhang, Y.; Chickenyen, S.; Wang, Y.; Zhou, F. *Biochemistry* **2007**, 46, 9270. DOI: 10.1021/bi700508n
29. A. Awasthi, A.; Matsunaga, Y.; Yamada, T. *Exp. Neurol.* **2005**, 196, 282. DOI: 10.1016/j.expneurol.2005.08.001
30. Y. Matsunaga, Y.; Fujii, A.; Awasthi, A.; Yokotani, J.; Takakura, T.; Yamada, T.; *Regul. Pept.* **2004**, 120, 227. DOI: 10.1016/j.regpep.2004.03.013
31. Liao, M.Q.; Tzeng, Y.J.; Chang, L.Y.; Huang, H.B.; Lin, T.H.; Chyan, C.L.; Chen, Y.C. *FEBS Lett.* **2007**, 581, 1161. DOI: 10.1016/j.febslet.2007.02.026
32. Liu, R.; McAllister, C.; Lyubchenko, Y.; Sierks, M.R. *J. Neurosci. Res.* **2004**, 75, 162.
33. Du, X.T.; Wang, L.; Wang, Y.J.; Andreasen, M.; Zhan, D.W.; Feng, Y.; Li, M.; Zhao, M.; Otzen, D.; Xue, D.; Yang, Y.; Liu, R.T. *J. Alzheimer's Dis.* **2011**, 27, 401. DOI: 10.3233/JAD-2011-110476
34. Furlan, S.; Hureau, C.; Faller, P.; La Penna, G. *J Phys Chem B* **2010**, 114, 15119. DOI: 10.1021/jp102928h
35. Istrate, A. N.; Kozin, S. A.; Zhokhov, S. S.; Mantsyzov, A. B.; Kechko, O. I.; Pastore, A.; Makarov, A. A.; Polshakov, V. I. *Scientific Reports* **2016**, 6, 21734. DOI: 10.1038/srep21734
36. Zirah, S.; Rebuffat, S.; Kozin, S. A.; Debey, P.; Fournier, F.; Lesage, D.; Tabet, J.-C. *Int. J. Mass Spectrom.* **2003**, 228, 999. DOI: 10.1016/S1387-3806(03)00221-5
37. Ma, Q.-F.; Hu, J.; Wu, W.-H.; Liu, H.-D.; Du, J.-T.; Fu, Y.; Wu, Y.-W.; Lei, P.; Zhao, Y.-F.; Li, Y.-M. *Biopolymers*, **2006**, 83, 20. DOI: 10.1002/bip.20523
38. Li, J.; Lyu, W.; Rossetti, G.; Konijnenberg, A.; Natalello, A.; Ippoliti, E.; Orozco, M.; Sobott, F.; Grandori, R.; Carloni, P. *J. Phys. Chem. Lett.* **2017**, 8, 1105. DOI: 10.1021/acs.jpclett.7b00127